

Integrated Preconcentration SDS–PAGE of Proteins in Microchips Using Photopatterned Cross-Linked Polyacrylamide Gels

Anson V. Hatch, Amy E. Herr, Daniel J. Throckmorton, James S. Brennan, and Anup K. Singh*

Biosystems Research Department, Sandia National Laboratories, Livermore, California 94551

The potential of integration of functions in microfluidic chips is demonstrated by implementing on-chip preconcentration of proteins prior to on-chip protein sizing by sodium dodecyl sulfate–polyacrylamide gel electrophoresis (SDS–PAGE). Two polymeric elements—a thin ($\sim 50 \mu\text{m}$) size exclusion membrane for preconcentration and a longer ($\sim \text{cm}$) porous monolith for protein sizing—were fabricated in situ using photopolymerization. Contiguous placement of the two polymeric elements in the channels of a microchip enabled simple and zero dead volume integration of the preconcentration with SDS–PAGE. The size exclusion membrane was polymerized in the injection channel using a shaped laser beam, and the sizing monolith was cast by photolithography using a mask and UV lamp. Proteins injected electrophoretically were trapped on the upstream side of the size exclusion membrane (MW cutoff $\sim 10 \text{ kDa}$) and eluted off the membrane by reversing the electric field. Subsequently, the concentrated proteins were separated in a cross-linked polyacrylamide monolith that was patterned contiguous to the size exclusion membrane. The extent of protein preconcentration is easily tuned by varying the voltage during injection or by controlling the sample volume loaded. Electric fields applied across the nanoporous membrane resulted in a concentration polarization effect evidenced by decreasing current over time and irreproducible migration of proteins during sizing. To minimize the concentration polarization effect, sieving gels were polymerized only on the separation side of the membrane, and an alternate electrical current path was employed, bypassing the membrane, for most of the elution and separation steps. Electrophoretically sweeping a fixed sample volume against the membrane yields preconcentration factors that are independent of protein mobility. The volume sweeping method also avoids biased protein loading from concentration polarization and sample matrix variations. Mobilities of the concentrated proteins were log–linear with respect to molecular weight, demonstrating the suitability of this approach for protein sizing. Proteins were concentrated rapidly ($< 5 \text{ min}$) over 1000-fold followed by high-resolution separation in the sieving monolith. Proteins with concentrations as low as 50 fM were detectable with 30 min of preconcentration time. The integrated preconcentration–sizing approach facilitates analysis of low-

abundant proteins that cannot be otherwise detected. Moreover, the integrated preconcentration–analysis approach employing in situ formation of photopatterned polymeric elements provides a generic, inexpensive, and versatile method to integrate functions at chip level and can be extended to lowering of detection limits for other applications such as DNA analysis and clinical diagnostics.

The advent of microfluidic chips has enabled miniaturization of many biochemical techniques resulting in faster and less expensive analysis using much smaller amounts of sample and reagents. Microfluidic devices have in many ways revolutionized the analytical capabilities available for chemistry, biology, and medicine. Microfluidic devices allow analysis using minute amounts of samples (crucial when analyzing body fluids or expensive drug formulations), are fast, and enable development of portable systems. One of the biggest advantages offered by microfluidic chips, analogous to microelectronics chips, is the potential for seamless integration of functions at the chip scale. While great advances have been made in integrating some functions such as injection and analysis, in most cases, sample pretreatment is performed off-chip. Recently, approaches have been developed to incorporate functions such as sample cleanup, sample concentration, mixing, and reaction prior to analysis in microchips.^{1–3}

There are a number of reasons why sample concentration prior to analysis is a crucial step in development of multifunctional integrated microfluidic devices. First and foremost is that preconcentration of sample enables detection of trace or low-abundant species. This is of particular importance in many fields including clinical diagnostics, proteomics, forensics, environmental monitoring, and biodefense applications. A second motivation for preconcentration arises from the fact that micrometer dimensions of the fluidic channels lead to poorer sensitivities for optical detection than their conventional scale counterparts. Preconcentration not only improves detection sensitivity but also improves the reliability of analysis by significantly increasing signal-to-noise ratios. Another factor motivating preconcentration is the incongruity between available sample volume and the volume typically used

* To whom correspondence should be addressed. E-mail: aksingh@sandia.gov.

- (1) Auroux, P. A.; Iossifidis, D.; Reyes, D. R.; Manz, A. *Anal. Chem.* **2002**, *74*, 2637.
- (2) Reyes, D. R.; Iossifidis, D.; Auroux, P. A.; Manz, A. *Anal. Chem.* **2002**, *74*, 2623.
- (3) Vilckner, T.; Janasek, D.; Manz, A. *Anal. Chem.* **2004**, *76*, 3373.

for analysis in microfluidic chips. Practical constraints on sample loading limit the minimum volume of sample inserted into a chip to the order of $\sim 1 \mu\text{L}$ while the volume typically analyzed is on the order of $\sim 1 \text{ nL}$. Hence, analytes in a sample can be concentrated up to 1000-fold without requiring additional sample.

Reported sample preconcentration methods can be categorized into many groups including surface-binding, electrokinetic equilibrium, and porous membrane techniques based on the mechanisms used. Surface-binding techniques such as solid-phase extraction or affinity columns use sample adsorption to surfaces for concentration and a solvent or surface property change for elution.^{4–6} Electrokinetic equilibrium techniques concentrate sample by bringing species transport to a local equilibrium state electrokinetically, and examples include isoelectric focusing^{7–9} and field amplified sample stacking or isotachopheresis.¹⁰ Approaches have also been developed that rely on the concept of size-based exclusion to concentrate macromolecules using a porous membrane that excludes species of interest from the membrane pores.^{11–13} Each of these approaches has its own advantages and drawbacks. For example, sample stacking methods require insertion and maintenance of multiple buffer zones and can be difficult to implement with samples of unknown conductivity. Affinity-based preconcentration requires a change in buffer conditions for elution. A size exclusion- or filtration-based approach is arguably the easiest to implement as this approach avoids complications of specifically arranging zones of buffer and reagents or the need for selective binding and release of analytes while offering high sample capacities with concentration factors of > 1000 -fold. However, a filtration-based approach does require placement of nanoporous membranes inside specific channels. Khandurina et al. demonstrated a size exclusion approach for concentrating DNA¹³ and more recently for concentrating proteins,¹¹ wherein a silicate membrane was deposited between the glass cover plate and silicon substrate of a microchip. While a 600-fold signal increase was reported for proteins electrophoretically driven against the silicate membrane, the authors reported that (1) the chips were hard to fabricate in a reproducible manner, (2) the silicate membrane often had defects adversely affecting the concentration, and (3) anomalous transport from ion effects were observed, particularly with longer preconcentration times. Recently, Wang et al. reported a novel preconcentration technique with up to 1 million-fold concentration of proteins in $\sim 3 \text{ h}$ using a nanofluidic filter; however, this approach requires fabrication of micro- and nanochannels in the same chip.¹⁴

To integrate different analysis functionalities on-chip, our group^{12,15–18} as well as others^{6,19–21} have developed facile and rapid

methods for in situ fabrication of polymer structures in microchips by photopolymerization. In this approach, microchannels are filled with monomer solution including a photoinitiator. The polymerization is initiated by UV light, and using a mask or a shaped beam, the polymerization is restricted to UV-exposed regions. The ability to photopattern allows casting of polymers with different properties in different regions of the chip enabling seamless integration of multiple functions. Song et al. developed an electrophoretic concentrator using a nanoporous polymer membrane laser-patterned at the junction of a simple cross channel.¹² In this report, we describe the formation of an integrated system that uses two types of polymer structures—one containing nanopores to allow size-based concentration of proteins and the other containing larger pores for sieving of proteins. The two polymeric structures were formed contiguously to allow seamless integration of preconcentration with separation. As reported previously by Foote et al.,¹¹ nonlinear concentration factors and lack of reproducibility are problematic with a membrane-based approach to preconcentration. This behavior results from concentration polarization that can lead to sample destacking. In the pores of a size exclusion membrane, the thickness of the electrical double layer (EDL) can be on the same order of magnitude as the pore radius. For a negatively charged membrane such as glass or polyacrylamide, this results in selective enrichment of cations in the pores. In the absence of an applied electric field, a boundary potential (Donnan potential) exists between bulk and the membrane in counterbalance to unequal concentrations of ions. When an applied electric field is superimposed, concentration polarization results where concentrations of ions increase on the cathodic side and decrease on the anodic side. The steep concentration gradients in the depleted concentration polarization zone results in diffusion-limited transport of ions. This leads to a drop in current as a function of time upon application of the external electric field. At the diffusion limit, the current reaches a steady value referred to as “limiting current”. Localized increase in ion concentrations lead to sample destacking and other nonlinear effects resulting in band-broadening and irreproducible migration over time. Methods are described that helped to minimize concentration polarization and achieve reproducible results. We also introduce a fixed-volume loading approach that resulted in highly reproducible concentration factors by avoiding biasing by concentration polarization and sample matrix variations. The concentration factors with fixed-volume loading were also independent of protein mobilities. The successful integration of preconcentration with protein sizing is demonstrated by rapid, > 1000 -fold preconcentration of representative proteins and subsequent separations that exhibit the expected log–linear dependence of mobility on molecular weight.

- (4) Broyles, B. S.; Jacobson, S. C.; Ramsey, J. M. *Anal. Chem.* **2003**, *75*, 2761.
- (5) Jemere, A. B.; Oleschuk, R. D.; Ouchen, F.; Fajuyigbe, F.; Harrison, D. J. *Electrophoresis* **2002**, *23*, 3537.
- (6) Yu, C.; Davey, M. H.; Svec, F.; Frechet, J. M. J. *Anal. Chem.* **2001**, *73*, 5088.
- (7) Li, Y.; DeVoe, D. L.; Lee, C. S. *Electrophoresis* **2003**, *24*, 193.
- (8) Cabrera, C. R.; Yager, P. *Electrophoresis* **2001**, *22*, 355.
- (9) Huang, T. M.; Pawliszyn, J. *Electrophoresis* **2002**, *23*, 3504.
- (10) Wainright, A.; Williams, S. J.; Ciambrone, G.; Xue, Q. F.; Wei, J.; Harris, D. *J. Chromatogr., A* **2002**, *979*, 69.
- (11) Foote, R. S.; Khandurina, J.; Jacobson, S. C.; Ramsey, J. M. *Anal. Chem.* **2005**, *77*, 57.
- (12) Song, S.; Singh, A. K.; Kirby, B. J. *Anal. Chem.* **2004**, *76*, 4589.
- (13) Khandurina, J.; Jacobson, S. C.; Waters, L. C.; Foote, R. S.; Ramsey, J. M. *Anal. Chem.* **1999**, *71*, 1815.
- (14) Wang, Y. C.; Stevens, A. C.; Han, J. *Anal. Chem.* **2005**, *77*, 4293–4299.

- (15) Throckmorton, D. J.; Shepodd, T. J.; Singh, A. K. *Anal. Chem.* **2002**, *74*, 784–789.
- (16) Herr, A. E.; Singh, A. K. *Anal. Chem.* **2004**, *76*, 4727–4733.
- (17) Han, J. Y.; Singh, A. K. *J. Chromatogr., A* **2004**, *1049*, 205–209.
- (18) Song, S.; Singh, A. K.; Shepodd, T. J.; Kirby, B. J. *Anal. Chem.* **2004**, *76*, 2367.
- (19) Beebe, D. J.; Moore, J. S.; Yu, Q.; Liu, R. H.; Kraft, M. L.; Jo, B. J.; Devadoss, C. *Proc. Natl. Acad. Sci. U.S.A.* **2000**, *97*, 13488.
- (20) Brahmasandra, S. N.; Ugaz, V. M.; Burke, D. T.; Mastrangelo, C. H.; Burns, M. A. *Electrophoresis* **2001**, *22*, 300–311.
- (21) Moorthy, J.; Mensing, G. A.; Kim, D.; Mohanty, S.; Eddington, D. T.; Tepp, W. H.; Johnson, E. A.; Beeke, D. J. *Electrophoresis* **2004**, *25*, 1705.

EXPERIMENTAL SECTION

Reagents. *N,N*-methylene bisacrylamide powder and solutions of 3-(trimethoxysilyl)propyl methacrylate (98%), 40% acrylamide, and 30% (37.5:1) acrylamide/bisacrylamide solutions were from Sigma (St. Louis, MO). Caution: monomeric acrylamide compounds are neurotoxins that can be absorbed through the skin or inhaled (powder) and should only be handled with appropriate precautions. The 10× Tris/glycine/SDS electrophoresis buffer (25 mM Tris, 192 mM glycine, 0.1% SDS, pH 8.3 at 1×) was from BioRad (Hercules, CA). The water-soluble photoinitiator 2,2'-azobis[2-methyl-*N*-(2-hydroxyethyl)propionamide] (VA-086) was from Wako Chemicals (Richmond, VA). Glacial acetic acid was also from Sigma. The Alexa Fluor 488-labeled proteins parvalbumin (PA), trypsin inhibitor (TI), ovalbumin (OA), and bovine serum albumin (BSA), the seven-protein BenchMark fluorescent protein standard, and NuPAGE sample reducing buffer were from Invitrogen (Carlsbad, CA). IgG antibody (antiCRP) (US Biological) was labeled with Alexa Fluor 488 protein labeling kit (Invitrogen) according to manufacturer's instructions. A stock solution of 22% (15.7:1) acrylamide/bisacrylamide was prepared by combining bisacrylamide powder, 40% stock acrylamide, and water and filtering with a 0.2- μ m syringe filter.

Chip Fabrication. Previously described photolithography, wet etching, and bonding techniques were used to fabricate microchips from Schott D263 glass wafers (4-in. diameter, 1.1-mm thickness; S. I. Howard Glass Co., Worcester, MA).¹⁵ The channels were \sim 40 μ m deep \times \sim 100 μ m wide. To anchor gels to the channel walls, microchannels were first coated with acrylate-terminated self-assembled monolayers as described previously.¹⁴ The channels were conditioned with 1 M NaOH, rinsed with deionized water, and purged by vacuum. The dried channels were loaded with a sonicated and degassed 2:3:5 (v/v/v) mixture of 3-(trimethoxysilyl)propyl methacrylate, glacial acetic acid, and deionized water. The mixture was incubated for 30 min to deposit a packed silane monolayer, rinsed with a 3:7 mixture of acetic acid and water, rinsed with deionized water, and purged by vacuum.

To fabricate the size exclusion membrane, chips were loaded by capillary action with a degassed solution of 22% (15.7:1) acrylamide/bisacrylamide containing 0.2% (w/v) VA-086 photoinitiator. The inlet well was cleared, and then each well was filled with 1 μ L of monomer/photoinitiator solution, capped with tape to prevent evaporation, and equalized for 5 min to eliminate pressure-driven flow. The narrow \sim 50- μ m membrane was photopolymerized with a 15-s exposure to a rectangular shaped 355-nm laser beam using an optical setup described previously.^{12,18} The unpolymerized monomer solution was purged from the channels by vacuum. The empty channels were then rinsed with either buffer or buffered monomer solution used to form the sieving gel. The sieving gel was photopolymerized after membrane formation by loading a degassed solution of 8% (37.5:1) acrylamide/bisacrylamide and 0.2% (w/v) VA-086 in 1× Tris/glycine/SDS buffer into the separation channel. Chips were exposed to light from a 100-W 365-nm lamp for 5 min to photopolymerize the separation gel. Chips were stored submerged in buffer at 5 °C when not in use.

Apparatus. A custom manifold similar to that described by Renzi et al.²² was used to mount the chip over the optical setup,

supply sample and reagents to the chip, and interface power supply leads. An aluminum backing plate secured the chip against a custom machined Delrin (DuPont) sample tray with O-ring compression fittings that sealed individual sample reservoirs over the chip inlets. The centers of the aluminum backing plate and sample tray were open for optical access to the chip. Programmable high-voltage power supplies with current monitoring capabilities were fabricated in-house.²² A custom high input resistance (10^{11} Ω) voltage probe was used to track node voltages at channel intersections during chip operation while imposing a negligible load on the circuit. Microscope images were captured by a 1300 \times 1030 pixel, Peltier-cooled interline CCD camera (CoolSnap HQ, Roper Scientific, Trenton, NJ) mounted on an inverted epifluorescence microscope (IX-70, Olympus, Melville, NY). The images presented illustrate qualitative chip behavior; spatial nonuniformities in the excitation and collection efficiencies of the optical system were not corrected. Electropherograms were generated using an argon ion laser (Melles Griot, Carlsbad, CA) beam (488-nm) with a frequency modulated (220-Hz mechanical chopper) for excitation. Epifluorescence optics with a 40× objective and a Hamamatsu H5784 photomultiplier tube (PMT) were used for detection. The PMT signal was demodulated using a lock-in amplifier (Stanford Research Systems, Sunnyvale, CA). The demodulated PMT signal and voltage probe readings were captured using a data acquisition interface (6020E DAQPad, National Instruments, Austin, TX) controlled by a laptop and a custom LabVIEW (National Instruments) program.

In initial experiments, sample was loaded directly from the sample (S = ground) reservoir to the preconcentration waste (PW = 300 V) reservoir (see Figure 1) to trap and preconcentrate proteins at the membrane ($E = 135$ V/cm). Sample was followed up with loading buffer for 30 s (LB = 0, PW = 300 V) to clean up protein remaining in the short segment leading to the membrane. Trapped sample proteins were subsequently eluted and separated in a single step toward the buffer waste (BW = 1200 V) reservoir with the buffer (B) reservoir grounded (other wells = float, $E = 320$ V/cm). To reduce concentration polarization in later experiments, fields were applied across the membrane for only 10 s for elution (B = ground, BW = 1200 V) and the elution was also pinched so that 1/3 of the current was from LB (set at 120 V in this case). For the remainder of the separation, LB was grounded instead of B so that the applied field bypassed the membrane. For volume loading experiments, sample proteins were first loaded into a holding reservoir by applying the field between S and load waste (LW) reservoirs (S = ground, LW = 500 V) rather than loading directly from sample toward the membrane. The protein in the sample loop was then swept to the membrane (LB = ground, PW = 300 V).

Quantifying Performance. The peak areas in all cases were normalized by elution time (peak area/elution time). Concentration factors were determined by normalizing the electropherogram peak areas by corresponding peaks from control tests (preconcentrated peak area/control peak area). The control data were generated with a standard T-injection using a chip fabricated without the preconcentration membrane. Calculations of theoretical plates (N) were based on the elution time of the peak center

(22) Renzi, R. F.; Stamps, J.; Horn, B. A.; Ferko, S.; VanderNoot, V. A.; West, J. A. A.; Crocker, R.; Wiedenman, B.; Yee, D.; Fruetel, J. A. *Anal. Chem.* **2005**, *77*, 435.

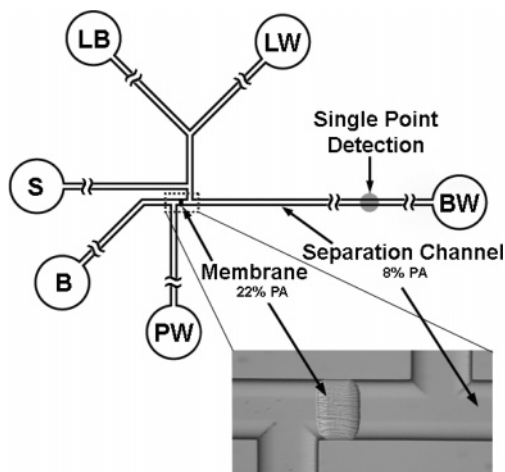


Figure 1. Chip design for integrated preconcentration and SDS–PAGE separations. The inset shows a bright-field image of a photopolymerized size exclusion membrane (visible due to light scattering) positioned in the offset-T junction. A polyacrylamide sieving monolith is photopolymerized in the separation channel contiguous with the size exclusion membrane. Proteins are detected at a fixed point in the separation channel (1 cm from the membrane). The wells are labeled as follows: sample (S), buffer (B), preconcentration waste (PW), buffer waste (BW), load buffer (LB), and load waste (LW).

(t_e) and the full elution width at half-maximum peak height (w) according to the equation, $N/m = 5.545(t_e/(wL))$, where L is the 1-cm length of separation before the detection point. Separation resolution (S_r) between a pair of peaks was based on the difference in their respective peak elution times and sum of their peak widths according to the relationship, $S_r = 1.18(t_{e2} - t_{e1})/(w_1 + w_2)$. Peak areas and widths were calculated using software developed in-house.

RESULTS AND DISCUSSION

Fabrication and Characterization of Size Exclusion Membrane and Sieving Monolith. Both the size exclusion membrane and the separation monolith were fabricated in situ within etched glass microchannels by UV-initiated photopolymerization (see Figure 1). These two types of polymers were different not only in porosity but also in geometry. The nanoporous polymer was cast as a thin membrane ($\sim 50 \mu\text{m}$) using projection optics to define a sheet of UV laser light while the sieving monolith ($\sim \text{cm}$ in length) was formed using a contact mask and UV flood illumination. The ability to pattern the polymeric elements contiguously in the same channel resulted in a zero dead volume integration of the protein preconcentration and separation functions. Continuity between the two polymeric structures avoids band-broadening resulting from flow variations due to differences in ζ potential and tortuosity in the open and polymer-filled segments.²³ The resolution of polymeric elements in channels is determined by the photopatterning technique used to fabricate them. The preconcentration membrane had 5–10-fold higher electrical resistance than the separation polymer based on current and voltage probe measurements at nodes on either side of the T-junction ($R = V/I$). To minimize the voltage drop across the membrane and thereby retain a high field for separation, the preconcentration membrane was fabricated with a short axial length ($50 \mu\text{m}$) compared to the separation

monolith ($> 15 \text{ mm}$). While projection lithography enables fabrication of features having dimensions of $10 \mu\text{m}$ or less (dependent on the wavelength and the numerical aperture of the focusing lens),²⁴ mechanical robustness constraints and ease of fabrication led to the choice of a slightly larger minimum membrane dimension. The separation polymer monolith does not require high resolution and was made by contact photolithography where resolution, dependent on the wavelength of light used and the thickness of the glass wafer, was $\sim 60 \mu\text{m}$ in our case.²⁵

Cross-linked polyacrylamide, a standard sieving material used for protein sizing, was the polymer of choice not only for the protein sieving monolith but also for the size exclusion membrane, as polyacrylamide is hydrophilic, inert, shows minimal nonspecific adsorption of proteins, and can be polymerized in an aqueous buffer avoiding organic solvents that may leave a residual or suffer from incompatibility with chip materials or biological samples. Moreover, adjusting the pore size of acrylamide gels is straightforward with a direct dependence of pore size on the percentage of monomer components.^{25–27} The sieving polymer used in this study was an 8% polyacrylamide (2.5% C) solution tailored for size-based separation of proteins in the molecular mass range of ~ 20 –200 kDa.

Much higher percentages of total monomer (%T) and cross-linker (%C) were necessary to fabricate preconcentration membranes that have pore sizes small enough to exclude a wide range of proteins ($> 10 \text{ kDa}$), but the pores must also maintain permeability to buffer ions. Optimization of the appropriate size exclusion cutoff characteristics required empirical characterization of gels from 15 to 27%T and 5–9%C. In addition to size exclusion, the choice of pore size was motivated by desires to limit the electrical resistance of the membrane that (1) contributes to Joule heating and (2) lowers the applied fields available to neighboring channels due to voltage division. The membrane also contributes to concentration polarization, which is lessened with compositions having a lower gel percentage. Membranes consisting of 22%T/6%C were chosen for the work presented here as pore sizes were empirically determined to be close to the size exclusion cutoff for proteins of $> 10 \text{ kDa}$ (data not shown). With 20%T/5%C membranes, a significant fraction of protein reaching the membrane became entangled within the membrane. All gels tested were optically clear except for a 27%T/9%C gel, presumably because the high cross-linker percentage resulted in a different regime of polymerization where pore sizes have been shown to increase by raising the cross-linker percentage too high.²⁸ A bright-field micrograph of an integrated chip with a photopolymerized size exclusion membrane and sieving gel is shown in Figure 1 (inset).

Preconcentration and SDS–PAGE. The layout of chip design used for different modes of preconcentration is shown in Figure 1. To concentrate and separate proteins, chip operations are similar to established protocols for offset-T injections except that a size exclusion membrane is positioned in the offset (Figure 1). During preconcentration, an electric field is applied across the

(24) Madou, M. *Fundamentals of Microfabrication*; CRC Press, New York, 1997.

(25) Holmes, D. L.; Stellwagen, N. C. *Electrophoresis* **1991**, *12*, 612.

(26) Holmes, D. L.; Stellwagen, N. C. *Electrophoresis* **1991**, *12*, 253.

(27) Chui, M. M.; Phillips, R. J.; McCarthy, M. J. *J. Colloid Interface Sci.* **1995**, *174*, 336.

(28) Margolis, J.; Wrigley, C. W. *J. Chromatogr.* **1975**, *106*, 204.

(23) Rathore, A. S.; Horvath, C. *Anal. Chem.* **1998**, *70*, 3069.

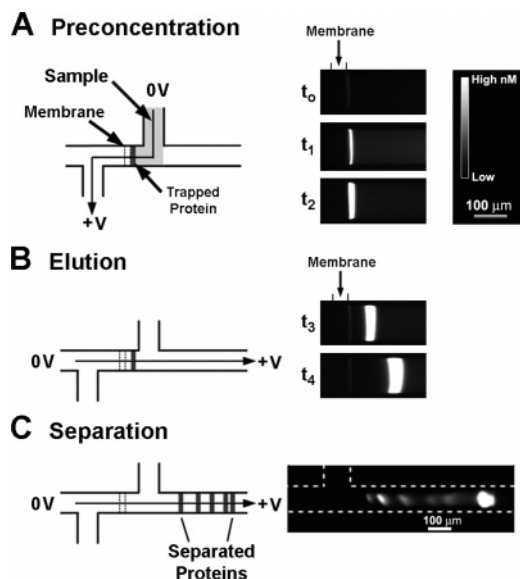


Figure 2. Preconcentration, elution, and separation of proteins. Schematic depicts the sequential process of protein pre-concentration (A), elution (B), and separation (C). The fluorescence micrographs show snapshots of the distribution of labeled protein (visible only after pre-concentration) at different time points of the integrated process. (A) During the pre-concentration step, an electric field drives the transport of protein SDS complexes toward the size exclusion membrane, where they become trapped and accumulate as long as the field is applied. The fluorescence micrographs show labeled BSA accumulating at the membrane ($t_0 = 0$ s, $t_1 = 30$ s, and $t_2 = 120$ s pre-concentration time). (B) Immediately following the pre-concentration step, the field across the membrane is reversed, redirecting proteins away from the membrane ($t_3 = 120.5$ s, $t_4 = 121$ s). (C) During SDS-PAGE, proteins migrate into the separation channel where they are size-separated. The lower fluorescent micrograph shows the separation of a seven-protein size ladder within a 1-mm distance of the membrane. Proteins begin separating almost immediately after field reversal as the separation monolith is immediately adjacent to the size exclusion membrane.

membrane between the sample (S) and pre-concentration waste (PW) reservoirs (S = ground, PW = +V, other leads = float), causing negatively charged protein/SDS complexes to migrate toward the membrane where they are trapped and concentrated. Fluorescence micrographs in Figure 2A show the accumulation of fluorescently labeled BSA at the membrane for different time points during the pre-concentration step. Once the desired level of pre-concentration is achieved, a separation step commences wherein the band of concentrated sample protein is eluted from the membrane and injected into the separation channel. Elution and injection are achieved by reversing the electrical field polarity across the membrane between the buffer (B) and buffer waste (BW) reservoirs (B = ground, BW = +V, other leads = float). Proteins cleanly elute from the membrane and are separated into distinct bands within a short distance from the membrane, as shown in the fluorescence micrographs in Figure 2B,C. Refinements to the protocol, including incorporation of additional channels and manipulation steps (discussed later), were made to clear sample from the loading channel, pinch injections, minimize concentration polarization, and give the option of fixed-volume sample loading.

Proteins ranging in size from 12 to 205 kDa were effectively trapped at the membrane and eluted cleanly as shown in Figure

2. Fluorescence imaging showed that proteins in this range did not permeate or become entangled within the membrane, but were instead concentrated within a narrow region immediately adjacent to the membrane surface. The protein eluted as a sharp band when the field was reversed, leaving a negligible trace of fluorescence indicating minimal fouling or nonspecific interactions with the polymeric elements used (Figure 2B). Unincorporated dye molecules present in trace quantities passed through the membrane, as was verified by imaging of fluorescein transport during pre-concentration (hence, the membrane could also be used for rapid sample cleanup, e.g., for removing unincorporated dye or for buffer exchange).

Concentration Polarization at the Nanoporous Size Exclusion Membrane. For the slightly basic conditions used in this work, hydrolysis of a small percentage of polymer amide bonds can be expected^{29,30} leaving negatively charged carboxylic groups on the polymer. With the fixed polymer charge and small pore sizes in the size exclusion membrane, the thickness of the EDL can be on the order of the pore radius. The negative surface charge and EDL overlap imparts partial cation selectivity to the membrane resulting in preferential enrichment of cations and exclusion of co-ions (anions). In the presence of an externally applied electrical field, the membrane selectivity for cations induces concentration polarization^{31,32} in the bulk solution on both sides of the membrane as illustrated in Figure 3A. At the anodic side of the membrane, counterions are depleted, and to maintain electroneutrality, total ion concentration decreases compared to the bulk. The decrease in ionic concentration in the boundary layer that extended well into the channel on the anode side, leading to a higher resistance, results in a net decrease in current as a function of time as shown in Figure 3B. The drop in current is exponential—an initial sharp decline is followed by attainment of a limiting nonzero value when cation concentration reaches equilibrium. At this point, electromigration of cations into the pores of the membrane is counterbalanced by replenishment from the anodic side of the channel by electromigration and diffusion. The concentration polarization effects were monitored by measuring resistance in different sections of the chip using a high-voltage probe (Figure 3A). It is evident that there is not a significant change in the resistance across the membrane or on the cathodic side. However, there is a significant increase in resistance with time on the anodic side of the membrane leading to a drop in current shown in Figure 3B. This polarization behavior was observed with newly fabricated chips exposed only to native Tris/glycine buffer (no SDS and no added protein) ruling out sample-related mechanisms such as clogging of the pores by protein (Figure 3B). The drop in current was more pronounced when SDS was added, but adding protein at the concentrations tested did not affect the rate of current drop. Current drops were only observed when field was applied across the membrane (e.g., with a fresh or equilibrated chip, electric currents were stable when fields were applied along paths that bypassed the membrane). A modest increase in local ionic strength was observed on the cathodic side of the membrane, which leads to a destacking effect

(29) Kleparnik, K.; Mikuska, P. *Electrophoresis* **2004**, *25*, 2139.

(30) Kurnekov, V. F.; Hartan, H. G.; Lohanov, F. I. *Russ. J. Appl. Chem.* **2001**, *74*, 543.

(31) Helfferich, F. J. *Am. Chem. Soc.* **1962**, *84*, 3237.

(32) Tallarek, U.; Leinweber, F. C.; Nischang, N. *Electrophoresis* **2005**, *26*, 3237.

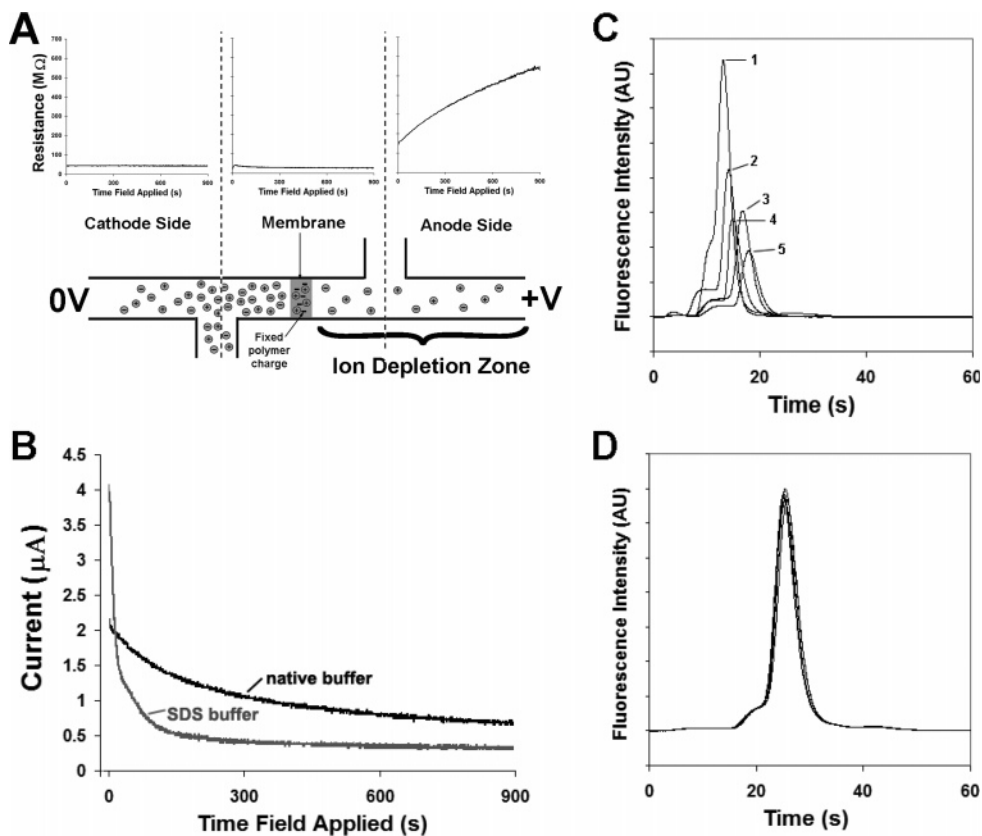


Figure 3. Concentration polarization effects arising from electric fields applied across the size exclusion membrane. (A) Illustration of concentration polarization caused by slight cation selectivity of the membrane. Depletion of ions resulted in the increase in resistance on the anode side of the membrane, which was coincident with a drop in current shown in (B). (B) Plotted are changes in electrical current observed as an electric field was applied across the membrane (B = ground, BW = +400 V, other leads = float) for 15 min (much longer than necessary for typical separations). The current dropped only when the fields were applied across the membrane and not when fields bypassed the membrane (e.g., S to BW). (C) Poor reproducibility was observed prior to minimization of concentration polarization effects. Shown are consecutive replicates of native PAGE separations of fluorescently labeled monoclonal IgG antibody. Large variations in concentration factor and elution time were observed due to concentration polarization effects. (D) Reproducibility was dramatically improved when bypassing the membrane during most of the separation step and when sieving gel was not polymerized in channels on the PW side of the membrane, shown here by five consecutive replicates obtained with the same preconcentration time and voltage used in (C) but with an altered elution protocol.

when the field is reversed for elution. The polarization gradually dissipates by diffusion after the applied field is removed.

Before modifications were made to resolve concentration polarization, irreproducible loading and separation of proteins were problematic as shown in Figure 3C. A chip that was initially equilibrated overnight was subjected to consecutive replicates of a preconcentration and separation protocol (identical applied voltages and times). The current during the preconcentration step dropped over the course of these experiments with a concentration polarization-induced drop in field strength on the cathode side that slowed the rate of protein loading. Thus, the total protein trapped at the membrane dropped substantially with each test, indicating that transport was reduced. The average resistance in the separation channel, measured during the separation phase, increased with consecutive testing. But there was also ion enrichment on that same side of the membrane during each preconcentration step. Both a depletion zone in the separation channel and enrichment more immediate to the membrane lead to destacking of proteins that is also shown in Figure 3C. The extent of protein loading and destacking was dependent on the magnitude and timing of applied fields and the dynamics of the localized gradients generated, which were complicated by the

reversal of fields across the membrane and along different paths during each cycle.

Similar behavior has been reported for both cross-linked and linear polymer DNA capillary electrophoresis sequencing gels.³³ Over the course of DNA sequencing runs, the current through the capillary has been reported to drop gradually as an ion depletion zone forms and expands within one end of the capillary. Left untreated, this effect has been shown to slow peak migration and reduce separation efficiency. The presence of large quantities of template DNA in CE experiments has also been shown to increase the propensity for ion depletion, resulting in more rapid drops in current.³⁴ The faster current drops are attributed to large negatively charged DNA templates being trapped at the edge of the gel that contribute to ion selectivity. A similar phenomenon occurred in the preconcentration chip presented in this work when SDS was added to the buffer. The increased rate of current drop (Figure 3B) was attributed to stacking of SDS micelles at the edge

(33) Bilenko, O.; Gavrilov, D.; Gorbovitski, B.; Gorfinkel, V.; Gouzman, M.; Gudkov, G.; Khozilov, V.; Khozikov, O.; Kosobokova, O.; Lifshitz, M. Luryi, S.; Stepoukhovitch, A.; Tcheravishnick, M.; Tyshko, G. *Electrophoresis* **2003**, *24*, 1176.

(34) Figeys, D.; Dovichi, N. J. *Chromatogr., A* **1995**, *717*, 113.

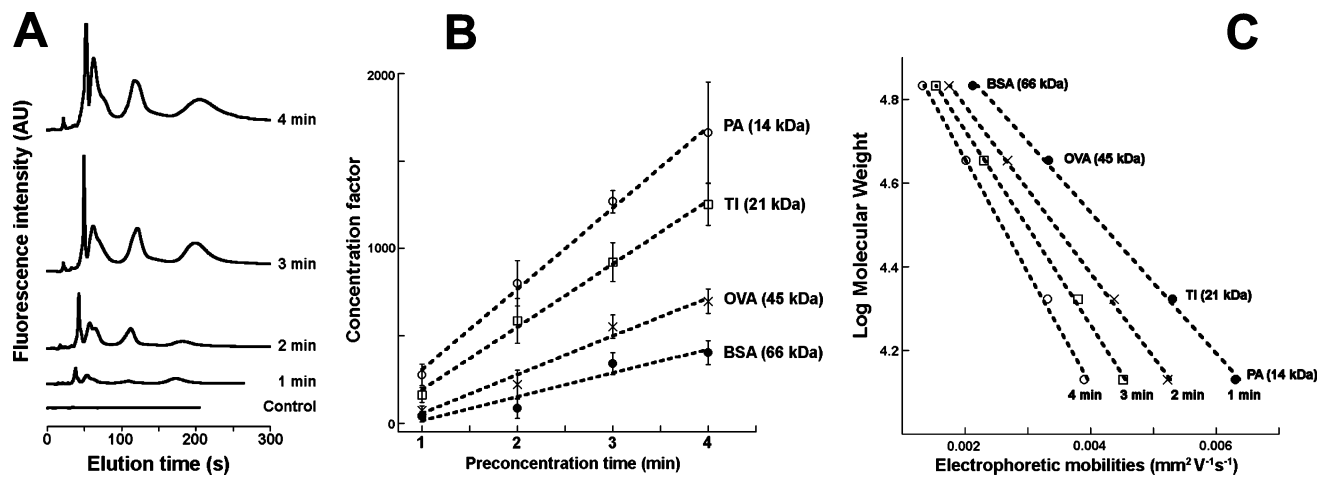


Figure 4. Preconcentration by direct loading of protein to the size exclusion membrane. (A) Electropherograms for different preconcentration times (1–4 min). The concentrated mixtures of four proteins were separated by SDS–PAGE. Without preconcentration, the proteins were just above the detector threshold (control). The peak heights increased in proportion to the time allowed for preconcentration (1–4 min) and in proportion to protein mobility. (B) The concentration factors for each protein are shown as a function of loading time. Proteins were concentrated 400- (BSA) to >1600-fold (PA) with 4 min of preconcentration. A linear trend was observed between concentration factors and loading time with the slope directly related to the mobility of SDS–protein complexes. (C) The plots for each preconcentration time show a linear correlation between log molecular weight and electrophoretic mobilities, which is necessary for protein sizing applications. The linear relationship was observed even when protein was concentrated over 1000-fold, although, with longer preconcentration times, separation mobilities and resolution were reduced.

of the membrane since the diameter of a pure SDS micelle is on the order of that for an SDS–protein complex (~5.7 and 6.2 nm, respectively, Samsó et al.³⁵). Further experiments with SDS below the critical micelle concentration (cmc) (5-fold reduction of SDS) indicated that SDS micelles, and not free SDS, contributed to the more pronounced current drop (data not shown). Based upon these observations, preconcentration with typical SDS–PAGE conditions would result in concentration polarization, which in turn leads to irreproducible elution times, thus requiring incorporation of steps to minimize charge polarization effects and ensure consistency.

Two steps were taken to minimize concentration polarization. First, the sieving gel that was initially cast on both sides of the membrane was limited to the separation side of the channel only. The channels on the preconcentration waste side of the membrane were instead left open and were filled with buffer during experiments. Localization of the sieving gel to the separation channel enabled buffer replenishment from the buffer well via bulk flow (EOF or pressure driven) on the side of the membrane having no gel. In accordance with the concentration polarization mechanism, the anodic side of the membrane would be depleted of ions during the preconcentration step. Continual replenishment of the buffer on the anodic side served to stabilize currents during preconcentration. Second, concentration polarization was minimized during the separation step by routing the electrical current to bypass the membrane during the majority of the separation step. To elute protein as a sharp band as shown in Figure 2, the field across the membrane was applied for a short time (~10 s) after which the membrane was bypassed by switching the grounded electrode from B to LB. Bypassing the membrane also proved to replenish ions depleted within the separation channel during the initial time in which the field was applied across the

membrane. For the geometry used, the peak shape of the eluted species was appreciably sharper if the duration of the applied elution field allowed the slowest migrating protein to move past the side channel (located ~100 μm away from the membrane), prior to electrical bypass of the membrane. Significantly improved reproducibility, Figure 3D, was obtained with the described modified approach implemented to minimize concentration polarization. The modified approach was used in all results reported in the sections below.

Two approaches were used to deliver proteins to the preconcentration membrane, here termed “direct loading” and “volume loading”.

Preconcentration with Direct Loading. In the direct loading approach, the electric field was applied across the membrane between S and PW reservoirs (S = ground, PW = +V). Thus, sample proteins were loaded directly from the sample well to the membrane. Figure 4 shows concentration factors at 1–4-min preconcentration time for BSA, PA, OVA, and TI. As is shown, concentration factors with 4-min preconcentration ranged from 400 for BSA to well over 1000 for the smaller proteins PA and TI. With direct loading, the concentration factor for each protein is a function of its electrophoretic mobility, the electric field strength, and time over which the field is applied. With SDS-coated proteins, mobility is size dependent. Thus, smaller proteins with higher mobility accumulate at the membrane faster than larger proteins and therefore exhibit higher concentration factors with direct loading. The electropherograms therefore give a skewed representation of relative protein concentrations present in the original sample, but the data can be compensated, if desired, by normalizing by elution time for each species. Such compensation would be inaccurate if relative protein mobilities during separation were different from those during loading (e.g., when a sieving gel is only present in the separation channel or if differences in sample

(35) Samsó, M.; Daban, J. R.; Hansen, S.; Jones, G. R. *Eur. J. Biochem.* **1995**, *232*, 818.

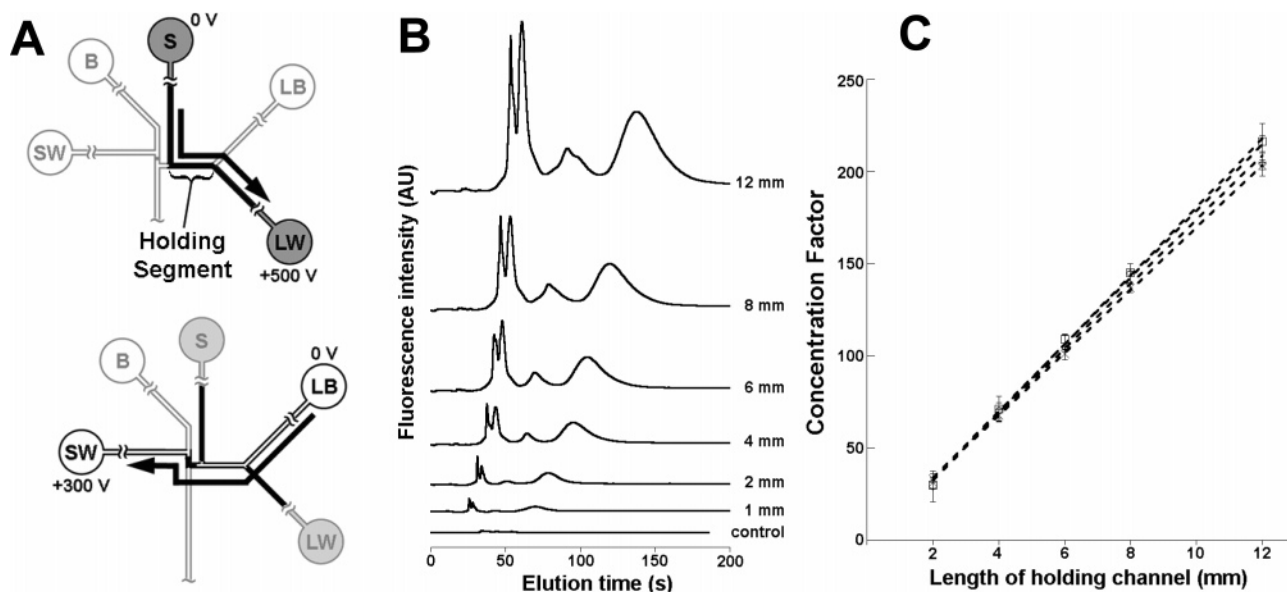


Figure 5. Preconcentration by swept-volume loading of protein. (A) In this implementation, sample is loaded into a holding volume defined by the holding channel length and cross-sectional area. Proteins in the holding channel are then swept to the nanoporous membrane. (B) Electropherograms for a concentrated mixture of four proteins size separated by SDS–PAGE. Without preconcentration, the proteins were just above the detector threshold (control). (C) The peak areas increased in direct proportion to the length of the sample holding segment (1–12 mm) that was swept (in this case, corresponding to the number of times a 1-mm holding section was swept). Concentration factors were >200 by sweeping 12 mm of holding segment. With volume loading, the concentration factors were independent of the mobility of SDS–protein complexes and were also more reproducible than for direct loading of protein (compare to Figure 4).

and buffer pH caused different mobilities during loading vs separation).

Concentration factors for each protein were roughly linear with respect to the time over which a given field strength was applied (within the time ranges tested). However, with this direct loading approach, variations in preconcentration factors for any given time were quite high even though currents were stable. The substantial variation in concentration factors is attributed to concentration polarization effects that can affect the sample loading channel with extensive use, as the data presented in Figure 4 were acquired from 50 separations run in immediate succession, but varied in order of preconcentration times. With long preconcentration times or continual testing, ion enrichment and associated changes in electrical resistance and pH could extend further and further into the sample loading channel.

As expected for SDS–PAGE, protein mobilities were found to be log–linear with molecular weight (Figure 4C). The integrated approach is thus useful for protein sizing applications. We also found that, with longer preconcentration times, protein mobilities were lower (similar to findings of Foote et al.,¹¹ but perhaps less pronounced) due to destacking of SDS micelles that are concentrated along with proteins, which reduces separation resolution. However, for a given preconcentration time, protein mobilities and sizing capabilities with SDS–PAGE were fairly consistent. Attempts were made to limit stacking of SDS micelles by lowering the concentration of SDS in the sample below the cmc and then adding a bolus of SDS micelles from a second sample reservoir (containing SDS above the cmc) after sample proteins were concentrated, but lower concentration factors and large deviations in results were observed for the conditions tested. Reduced elution mobilities and shifted elution times were not apparent at these concentration factors when no SDS was present (native PAGE experiments not reported here).

The detection limit with preconcentration was extended ~10 000-fold with 30 min of preconcentration time. Proteins were detected and resolved at concentrations as low as 50 fM (Supporting Information).

Preconcentration with Volume Loading. The volume loading approach is illustrated in Figure 5A. A holding channel segment was filled with sample (analogous to a sample loop injection) by applying a field between the S and load waste (LW) reservoirs (S = ground, LW = +V). Protein was then swept from the holding segment to the membrane by applying a field between the loading buffer (LB) and PW reservoirs (LB = ground, PW = +V). A defined volume of sample proteins is thereby concentrated at the membrane without dependence on protein mobility. The concentration factor is then not affected by the size and net charge of proteins, changes in pH, and ionic strength of the sample or by the electrical resistance, viscosity, and sieving properties of the loading channel.

With volume loading, the observed concentration factors were proportional to the swept volume of the sample holding loop (Figure 5C). Sufficient time was allowed to fully sweep the holding segment of the proteins studied so that concentration factors were independent of protein mobility. A 1-mm-length sample holding segment was loaded and swept 1–12 times to sweep different volumes of sample to the membrane. Extra preconcentration time was also allowed to ensure that the holding segment was fully swept of the largest species. The measured concentration factors were linear with swept volume and, as expected with volume loading, were equivalent for the four proteins, showing no dependence on protein mobility (Figure 5C). In this case, all proteins were concentrated >200-fold within 8 min. The volume loading method requires time to fill the holding segment with sample before drawing proteins toward the membrane, making the approach slower than that of direct loading. With the volume

Table 1. Number of Theoretical Plates and Separation Resolution with and without Preconcentration

volume loaded (mm)	separation efficiency (plates/m) (10^4)			resolution (S_r)	
	parvalbumin	trypsin inhibitor	ovalbumin	TI-OVA	PA-TI
control (0)	6.54	3.46	1.72	0.55	0.53
1	21.4	5.08	1.75	1.72	0.66
2	30.9	5.65	2	1.59	0.70
4	22.1	5.5	3.54	2.02	0.80
6	6.19	4.16	1.76	1.47	0.58
8	7.2	3.98	1.19	1.37	0.69
12	7.53	4.17	0.83	1.21	0.71

loading method, the standard deviations on the estimated concentration factors were lower than with the direct loading method (compare with Figure 4). The reduced variability in concentration factors was attributed to lower susceptibility to concentration polarization effects. With a fixed material volume that is fully swept to the membrane, net protein transfer is unaffected by concentration polarization-induced changes in the rate of material transfer. In contrast to the direct loading method, extension of the enrichment concentration polarization boundary layer along the path of loaded sample can be fully removed with the flushing of this path during the membrane bypass step.

Effect of Preconcentration on Separation Performance.

Integration of multiple functions and materials has the potential to adversely affect separation resolution and efficiency. For example, issues such as band dispersion during transfer from preconcentration to separation element or destacking due to ion enrichment can degrade separation performance. We compared the separation performance of the control condition (standard T-injection, no preconcentration membrane) to that with preconcentration using two metrics—the theoretical number of plates, N/m , and the separation resolution, S_r . Without preconcentration, the efficiency ranged from 1.72 to 6.54×10^4 plates/m for three proteins (Table 1). With preconcentration, there was an increase in efficiency for all proteins with the highest efficiency being 30.9×10^4 N/m for parvalbumin, 5.65×10^4 N/m for trypsin inhibitor, and 3.54×10^4 N/m for ovalbumin. The separation resolution improved upon preconcentration as well (S_r for trypsin inhibitor—ovalbumin more than doubled upon preconcentration; Table 1). The improvement in efficiency and resolution most likely results from focusing of sample into a narrower band at the size exclusion membrane compared to the width of the standard cross-injection. Separation performance was also comparable to previously reported values for chip and slab gel separations.¹⁶

CONCLUSIONS

We demonstrated a simple, inexpensive, and generic method for integrating functions and materials in a microchip using photopatterned polymeric elements. The approach was used to integrate preconcentration and SDS–PAGE of proteins using in situ polymerized polyacrylamide gels. The fabrication technique

allows the placement of a nanoporous preconcentration membrane contiguous with a cross-linked SDS–PAGE sieving gel that yields high-resolution separations. We achieved rapid protein preconcentration (<5 min) with concentration factors over 1000 (a 30-min concentration affords ~10 000-fold concentration factor) and separations that are useful for protein sizing applications. Proteins were detected and baseline resolved at concentrations as low as 50 fM with 30-min preconcentration time. Evidence showed that the size exclusion membrane trapped not only SDS-denatured proteins but also pure SDS micelles resulting in slower migration of eluted proteins at longer preconcentration times by destacking. Concentration polarization and ion depletion on the anode side of the membrane were also found to give poor reproducibility in concentration factors and elution times. Furthermore, the stacking of SDS micelles during preconcentration was found to dramatically enhance ion selectivity of the membrane leading to more pronounced concentration polarization. The likelihood of concentration polarization effects should therefore be considered even when using membranes presumed to rely on a size exclusion mechanism for trapping proteins (i.e., have very low surface charge density) particularly for typical SDS–PAGE conditions.

We found that reproducibility during SDS–PAGE was dramatically improved when concentration polarization was minimized by (1) using an open channel on the preconcentration-waste side of the membrane, which allows fluid flow to replenish buffer ions during the preconcentration step, and also by (2) bypassing the membrane during most of the separation step. The dependence of concentration factors on protein mobilities was also eliminated by using a swept-volume approach to loading protein. This approach showed much less deviation in concentration factors compared to direct loading of proteins by overcoming concentration polarization effects. The volume loading approach is much less dependent on sample conductivity, pH, viscosity, and other factors that could alter the rate of protein loading. The integrated approach is robust and should be useful for detecting low-abundance proteins, even those in complex sample matrixes, which cannot be analyzed by traditional sizing techniques.

ACKNOWLEDGMENT

We acknowledge Isaac Shokair for use of his data reduction software and Ronald Renzi for manifold fabrication. This work was supported by the National Institute of Dental and Craniofacial Research (Grant U01DE014961). Sandia is a multiprogram laboratory operated by Sandia Corp., a Lockheed Martin Co., for the United States Department of Energy under Contract DE-AC04-94AL85000.

SUPPORTING INFORMATION AVAILABLE

Additional information as noted in text. This material is available free of charge via the Internet at <http://pubs.acs.org>.

Received for review January 8, 2006. Accepted April 21, 2006.

AC0600454